UNIDIRECTIONAL SOLIDIFICATION OF DILUTE BINARY ALLOYS

by

SUDHAKAR D. BONDE

DEPARTMENT OF METALLURGICAL ENGINEERING

INDIAN INSTITUTE OF TECHNOLOGY KANPUR

JULY, 1976

UNIDIRECTIONAL SOLIDIFICATION OF DILUTE BINARY ALLOYS

A Thesis Submitted
In Partial Fulfilment of the Requirements
for the Degree of
MASTER OF TECHNOLOGY

by

SUDHAKAR D. BONDE

to the

DEPARTMENT OF METALLURGICAL ENGINEERING
INDIAN INSTITUTE OF TECHNOLOGY KANPUR

JULY, 1976

CERTIFICATE

This is to certify that this work "Unidirectional Solidification of Dilute Binary Alloys" has been carried out by S.D. Bonde under my supervision and has not been submitted elsewhere for a degree.

(Dr. M.N. SHETTY)
Assistant Professor
Department of Metallurgical Engineering
Indian Institute of Technology
Kanpur.

ACKNOWLEDGEMENTS

I wish to record my deep sense of gratitude to Dr. M.N. Shetty, for his valuable guidance, counsel, criticism of the work and his words of encouragement during the course of this investigation.

I am grateful to Dr. V.S. Arunachalam (Director) and Dr. M.L. Bhatia (Assistant Director), Defence Metallurgical Research Laboratory, Hyderabad, Mr. Deoras, Chief Metallurgist, H.S.L., Durgapur for extending the Electron-Probe Micro-Analyser facility.

I take this opportunity to thank Dr. V. Bansal, Dr. K.P. Gupta, Dr. A. Ghosh, Dr. M.L. Vaidya and Dr. M.S. Tyagi for their timely help and critical suggestions.

Thanks are due to Mr. K.P. Mukherjee for his assistance in melting the alloys used in this work and to Mr. R.N. Srivastava for excellent typing of manuscript.

Finally to my friends, I owe my gratitude for their help and co-operation in making stay here a pleasant experience.

(S.D. Bonde)

CONTENTS

LIST OF FIGURES

8. Phase diagram for Al-Al_3Ni system.

9. Microstructures of directionally solidified alloys at different velocities.

10. Inter-rod spacing (λ) as a function of growth rate (V).

11. Radius of curvature (ρ) as a function of growth rate (V).

12. Electron probe microanalysis.

13. Experimentally determined tip composition (C^S_{tip}) and interneedle region concentration as a function of growth rate (V) with constant thermal gradient (G) = 74°C/cm.

14. Parabolic coordinate system.

15. Tip concentration (C^S_{tip}) as a function of Peclet no. (P) for several velocities.

16. Tip undercooling (ΔT) as a function of Peclet no. (P) for several velocities.

~~17. Stress strain behaviour of Al-Al_3Ni composites~~

~~18. Microstructure of porous metal disc.~~

19. ~~Comparison of experimentally determined~~ C^S_{tip} with present model and zero constitutional supercooling theory.

ABSTRACT

Controlled solidification experiments were carried out on Al - 5.7 wt. % Ni eutectic alloys to investigate the effect of growth velocity on the solidification structures and variation of the tip composition of Al_3Ni precipitate needles. Optical metallography and electron probe micro-analysis were utilized to study the resulting microstructures and concentration distributions. Modified Ivanstov's analysis is applied by approximating the tip of a growing Al_3Ni precipitate to a paraboloid of revolution; to predict the compositional variations at the tip of the Al_3Ni precipitate. The observations are shown to be in a reasonable agreement with the predictions made.

CHAPTER 1

INTRODUCTION

During the solidification of an alloy of eutectic composition, solidification gets initiated at the mold walls and the resulting microstructure consists of small packets of eutectic structure randomly oriented with respect to one another. However if solidification is controlled and made to occur in one direction, then the microstructure will consist of these same packets of eutectic structure oriented parallel to one another and aligned along the direction of heat extraction. Such unidirectional solidification can be obtained by slowly withdrawing from a furnace a molten charge chilled at one end by a copper block. This creates a substantially uniaxial heat flow and a planar solid-liquid interface normal to the direction of charge movement.

The nature of the eutectic morphologies varies from one system to another. For example, one of the phases may exist as a continuous matrix, embedded with a second phase in the form of rods, lamella or globules etc. The variety of shapes that are possible illustrates the complex nature of the solidification process.

Here Al - 5.7 wt. % Ni eutectic is directionally solidified at different velocities and the effect of

growth velocity on solidification structure is studied. Calculations are made to predict the tip composition of whisker as it grows. The tip compositions are measured by Electron Probe Micro-analyser and the results are compared with the predictions.

This work aims to increase our understanding of directional solidification of Al-Al_3Ni eutectic, in the expectation that the results will have useful implications in the areas of casting and material preparation.

CHAPTER 2

BINARY EUTECTIC SOLIDIFICATION

2.1 Unidirectional Solidification

Unidirectional solidification is such that heat flows unidirectionally through one (plane) mold metal interface. There are two rules that must be followed to prevent equiaxed grain nucleation in the liquid. The melt temperature must be maintained above the liquidus and effective nucleating substrates must be removed from the melt. Melt temperatures and heat flow rates are easily controlled, and this is the basis for obtaining a columner casting. However some castings (cobalt base superalloys) require both thermal as well as chemistry control.

2.2 Heat Flow Control

The mold is suitably insulated so that after the molten metal is cast; most heat flow takes place through some bottom chill face. Since liquid superheat is rapidly lost via conduction to the chill face, it must be replenished as growth continues, and external heat is added to the system through it's sides from the exothermic compound comprising the mold. This method is the simplest and

cheapest of all practical techniques for ensuring predominantly unidirectional heat flow.

It is essential that the mold be in a vertical position so that S/L interface advances in a predominantly horizontal plane, which reduces the convective fluid motion and radial heat transfer usually associated with a vertical S/L interface. As the melt superheat gradually dissipates, the temperature gradient in the liquid gradually decreases until nucleation takes place and columnar growth ceases.

Conditions at the chill face are critical for proper unidirectional heat flow. (i) The chill plate must conduct the sensible heat out of the system and must have high conductivity. It may be water cooled. (ii) The surface of chill must be cleaned before each casting run so that resistance to heat flow by oxide layers is minimized. (iii) Mold should be securely clamped to the chill plate.

A major problem with this casting method is that both solidification rate and temperature gradient decrease with distance from the chill. Thus mechanical properties may get degraded due to cell or dendrite formation.

Controlling heat transfer rate by an external power source:

There are three methods by which controlled columnar growth can be obtained:

(i) By gradually lowering the power in the furnace that surrounds a fixed mold.

(ii) By withdrawing the mold and maintaining the power source in a fixed position.

(iii) By moving the heat source, keeping the mold in a fixed position.

The first method is called as "power down" growth control and the heat flow conditions are almost the same as that of in the case of exothermic molds.

The second method is "modified Stockbarger method" and can almost totally eliminate the variable structure disadvantage of the "power down" technique. This technique has the advantage that the thermal environment during freezing remains nearly constant throughout a large portion of freezing cycle. The basis of this method is that the furnace heat flow configuration requires a sharp temperature difference between the lower and upper furnace portions, which is provided by a baffle. The mold is gradually withdrawn through the baffle so that the S/L interface remains essentially parallel with the plane of the baffle. There will be some variation in structure with distance solidified, especially near the chill, but the upper extremetires of the casting should not have the variation in structure as in the previous casting methods. Columner castings can be

solidified almost four times faster with this method than with the power down techniques. The difficulties with this technique center around the high temperature which must be maintained about the mold to control freezing and the resulting mold problems.

The third method involves a stationary mold and a small movable zone heating source. The mold may be rotated during freezing to inhibit natural convection and thus heat transfer from the melt to the solid is decreased. The temperature gradient in the melt remains positive for a significantly longer time than in a conventional static casting. The consequent result is that the rate of crystal nucleation is decreased and castings can be grown with a much larger proportion of columner growth.

2.3 Eutectic Morphologies

From experimental observations, single phase materials can be divided into two groups according to their solidification characteristics; those that grow as non-faceted and other as faceted crystals. Jackson[1] showed that the type of growth depends on a factor α which is almost the entropy of melting and given by the relation[3]

$$\alpha = \frac{L_m \cdot \omega}{k \cdot T_m}$$

where L_m = Latent heat of melting

ω = Crystallographic factor (< 1)

k = Boltzmann's constant

T_m = Melting temperature

Most metals have α less than 2 and grow almost isotropically with no facets i.e. rough interface.

Eutectics can be classified in a similar manner into three groups.[1,2]

Rough – Rough ($\alpha < 2$ for both phases) e.g. Al-Ni, Al-Zn, Al-Cu and most of the metallic alloys.

(a) Lamellar

(b) Rod

(c) Cellular or colony – When third element as impurity is present it gives rise to supercooling ahead of interface and thus the plane interface breaks down into cellular.

Rough – Faceted ($\alpha > 2$ for one phase and $\alpha < 2$ for another phase) e.g. Al-Si where Al – Rough, Si – faceted

Fe-graphite[4]

Faceted – Faceted ($\alpha > 2$ for both phases) e.g. organic compounds, Si, Ge, Bi metal.

For eutectic alloys when precipitating phase has a low volume fraction there is a tendency to form rods and for higher volume fractions the tendency is for

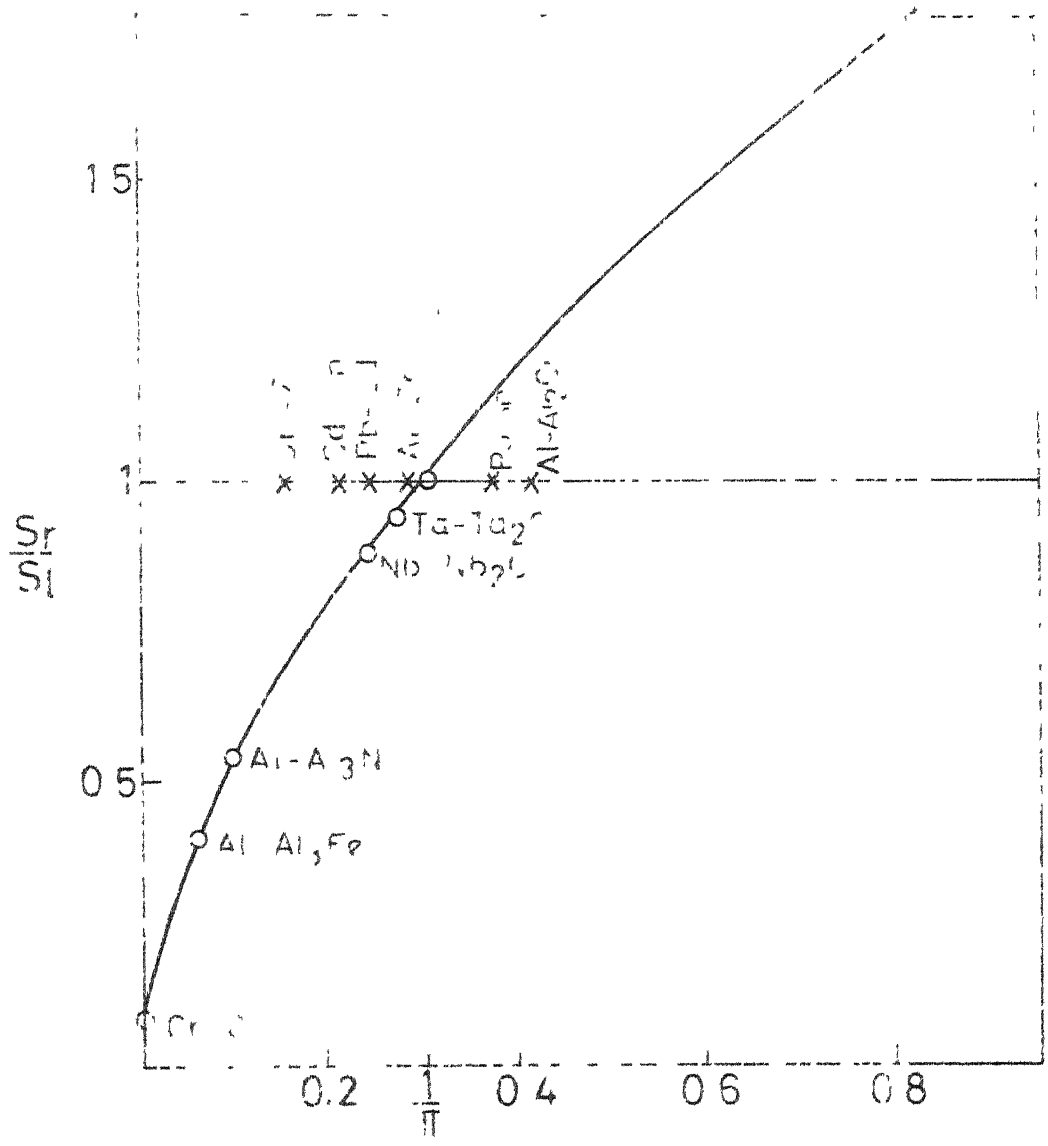

Fig. 1. The relative surface areas for lamellar eutectic arrangements (S_L), compared with those of rods (S_r), as functions of the volume proportions.

lamellae. It is generally accepted that this is controlled by interphase energy considerations[5] although under some conditions the solidification variables (growth rate; temperature gradient at S/L interface) can influence morphology. The preference for a given habit as determined by the simple geometric considerations is shown in Fig. 1. The surface area associated with a fibrous system (S_r) is very much sensitive to the volume proportions rising from zero to a maximum value of $\approx$ 0.8 when the rods would tend to make contact. On the other hand; the surface area of lamellar array (S_l) is independent of volume fraction since it is independent of lamellar thickness. If the interphase energies were the same for lamellae and rods we would only expect the lamellar arrangement at V_f greater than 0.3. However the lamellar habit is observed to persist to lower volume fractions and this has been attributed to the existence of preferred interphase habit planes with lower surface energies.[6] Thus we can see that the rod like arrangement is not expected at $V_f > 0.3$.

2.4 Mechanism of Eutectic Growth

The mechanism of eutectic growth in nonfaceted alloys has been treated by several authors.[1,2] A somewhat simplified version of the treatment of Jackson

and Hunt[2] for lamellar (plate like) eutectic growth is given here. Consider an alloy of eutectic composition C_E as shown in Fig. 2a; growing with a plane front except that the individual lamellae have slightly curved interfaces as sketched in Fig. 2b. As the α phase grows; it rejects B atoms into the liquid. Similarly the growing α phase rejects A atoms. Thus there is a slight build up of B atoms in front of α lamellae and depletion in front of the β lamellae as shown in Fig. 3a. If equilibrium pertains at the liquid-solid interface; there must now be an undercooling in front of the lamellae which depends on the amount of solute built up or depletion. This undercooling is

$$\triangle T_D = T_E - T_L$$

$$= m_L(C_E - C_L^*)$$

where $\triangle T_D$ = Undercooling due to solute diffusion; m_L = Liquidus slope, and C_L^* = Composition of the liquid at the location y on the S/L interface.

$\triangle T_D$ is marked on the phase diagram in Fig. 2a for a specific location y_1 in front of the α lamellae; and shown schematically in Fig. 2b with respect to y. It is to be noted that it can be either positive or negative.

Here the interface temperature T^* is assumed as constant as shown in Fig. 3b. This is true for most of

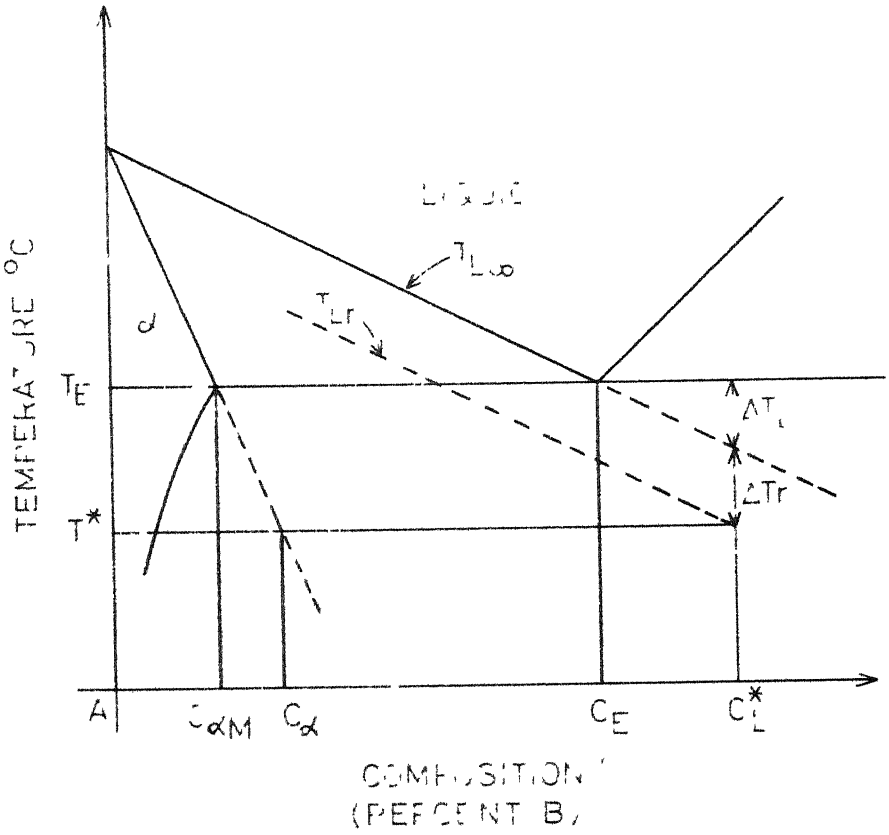

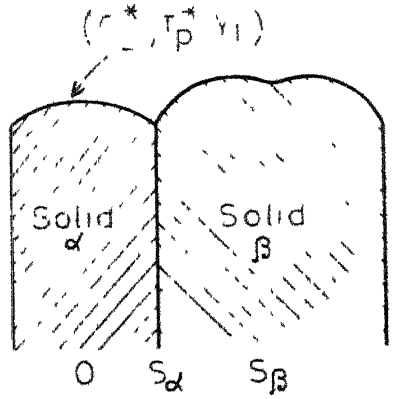

Fig. 2. Undercooling[illegible] composition C_L^* of a eutectic interface in front [illegible] ce [illegible]) applies.

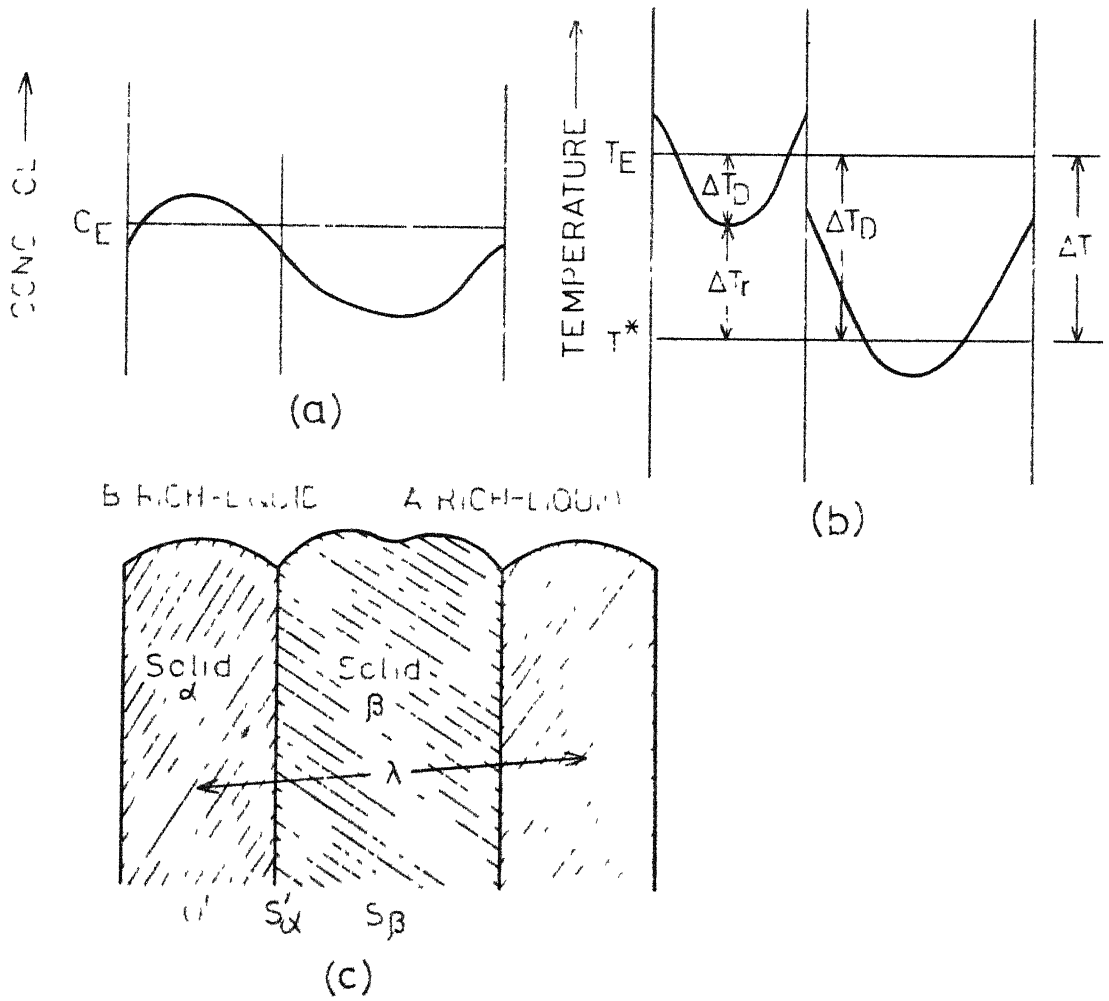

Fig. 3. Lamellar curvature in eute tic growth. (a) Solute concentration in the liqui at the interface; (b) Interfacial undercool: s ΔT_r, ΔT_D and ΔT; (c) Predicted sha amellar liquid-solid interface.

(From Ht

the nonfaceted eutectics because the curved surfaces of lamella in these eutectics usually deviate from a plane by less than a few microns. Hence, even if a temperature gradient exists in the growth direction, the variation in temperature from the leading to lagging part of a lamellae is negligible. The interface is maintained isothermal at T^* by the lamellae adjusting their radii of curvature locally. Then the total undercooling at the interface T is constant and is given by

$$\Delta T = T_E - T^*$$

$$= \Delta T_D + \Delta T_r$$

where $\Delta T_r = T_L - T_{Lr} = \frac{\sigma . T_E}{\rho . H . d_s}$

ΔT_r = undercooling due to radius of curvature

ρ = radius of curvature

H = heat of fusion

σ = S/L surface energy

d_s = solid density

T_{Lr} = liquidus temperature of singly curved surface of radius .

Fig. 2 shows this depression of the liquidus temperature at a location y_1 on the interface of the α phase of a

growing eutectic. The interface shape shown in Fig. 3c is that which produces the required values of T_r along the interface. It is to be noted that at the centre of the lamella ΔT_r is negative and so the ρ is also negative here. In case of rod morphology both the radius of curvature has to be taken into account.

The problem still remains is that which phase is the leading (controlling) phase for the above system and why? From the above description it is clear that here is the leading phase. The leading lamellae because of their ability to encroach on the retarded lamellae, will be the continuous phase.

2.5 Mechanism of Alternate Layer Formation

Tiller[7] proposed a mechanism for alternate layer formation. If a melt of eutectic composition is cooled to T_E and supercooled to produce an eutectic mixture. At some degree of supercooling nuclei of one phase will form in the liquid. The degree of supercooling at which this occurs will depend upon the number and type of hetrogeneous nucleation centers present in the liquid. As the crystals of this phase begin to grow, solute distributions will be build up ahead of them making the interface more greatly supercooled with respect to the second phase.

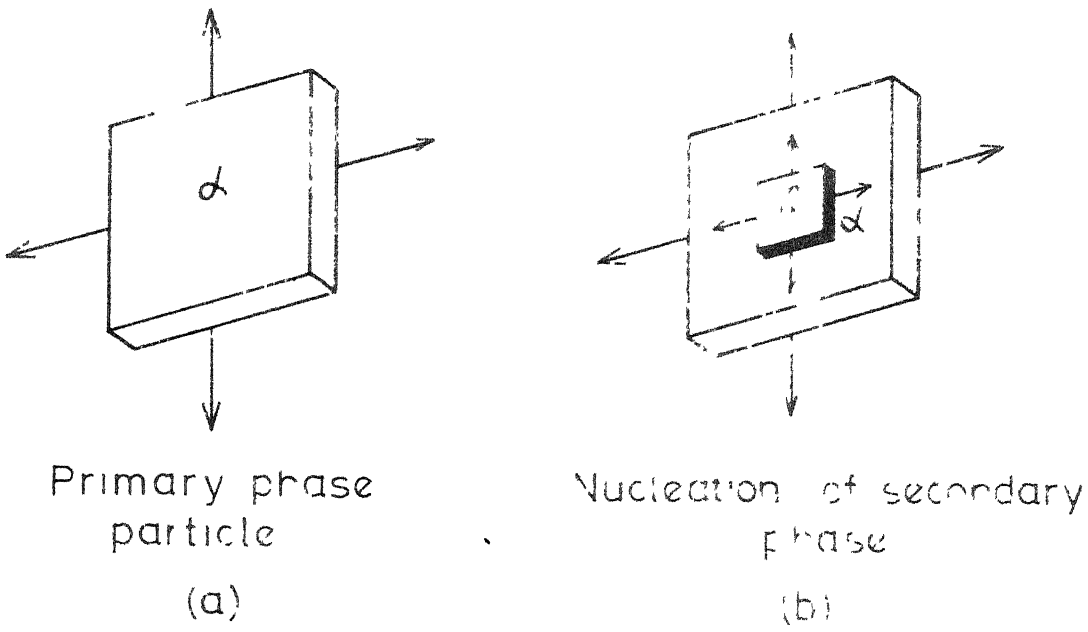

Fig. 4. Mechanism of alternate layer formation.

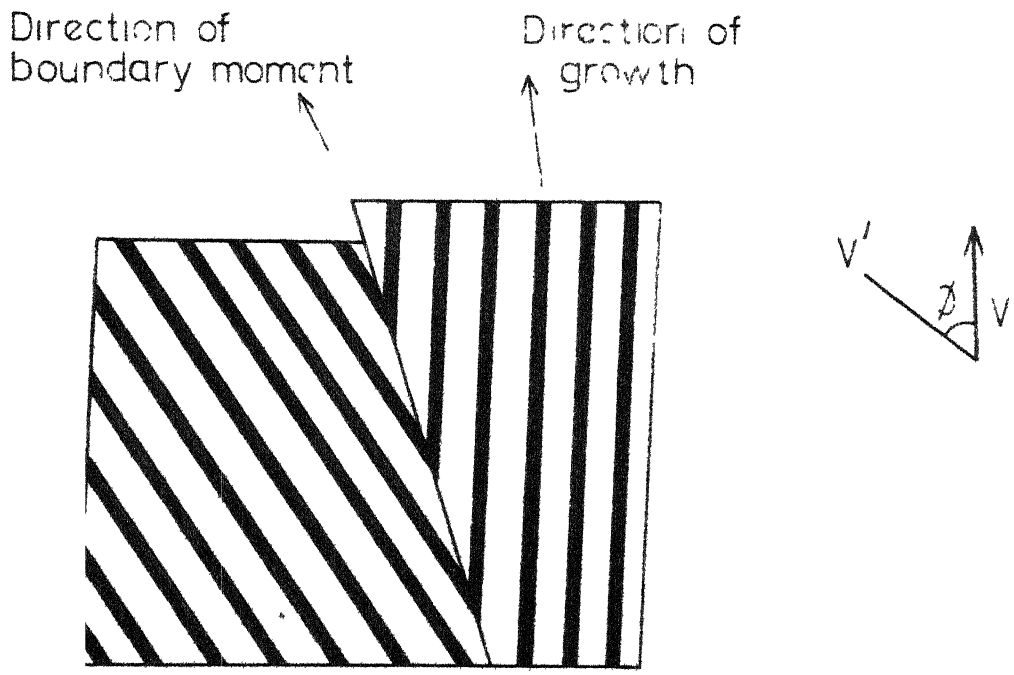

Fig. 5 ... opment of pr... ...tation of columnar ...s during ...ation.

The initial nuclei will probably grow as rods or plates as shown in Fig. 4a. If the primary phase serves as an effective nucleus for the second phase, the second phase will nucleate on the surface of the primary phase and absorb the supercooling. Fig. 4b illustrates the nucleation of the second phase on the face of the primary phase and the edgewise growth of this nucleus to absorb the supercooling. There are now two plates growing both edgewise and sidewise. The formation of new layers of alternate phase may readily occur by the overlap of one phase at the edge of the other. This overlapping process will probably occur at a higher interface temperature than independent nucleation of new layers on the exposed faces of the growing crystal and will therefore be the mechanism of layer formation. Thus a multilayered unit may be built by this overlapping mechanism.

2.6 Development of Preferred Orientation

The interfacial energy $\sigma\alpha\beta$ will depend upon the orientation of the $\alpha\beta$ interface plane and since the S/L interface is sensitive function of $\sigma\alpha\beta$, it can be shown how this will lead to a preferred orientation of the columner axis of the eutectic grains. Fig. 5 represents a bicrystal growing at some velocity V. The right hand grain has an orientation such that the preferred interface

between lamellae is perpendicular to the S/L interface orientation such that the preferred α-β plane makes an angle ϕ with the specimen axis. If the lamella boundaries follow the preferred plane, the lamellae are growing edgewise at the rate $V' = \frac{V}{\cos\phi}$ and the interface undercooling will be greater than the undercooling for the right hand grain due to this larger effective rate of freezing. Thus an interface step will be formed as illustrated in Fig. 5 which allows the right hand grain to encroach on the left hand grain and eliminate it from the specimen. In the final structure the surviving grains will be those having their specimen axis parallel to the preferred α-β plane.

2.7 Interspacing Adjustment

The relation between λ, V, ΔT can be expressed as[8]

$$\Delta T = A.V.\lambda + \frac{B}{\lambda}$$

where A, B are constants depending on particular alloy system, λ is interlamellar or interrod spacing and V is growth velocity.

For a fixed interface velocity V, one can have a range of ΔT and λ values as shown in Fig. 6. Experimental data, however, show no such ambiguity. For each V, one

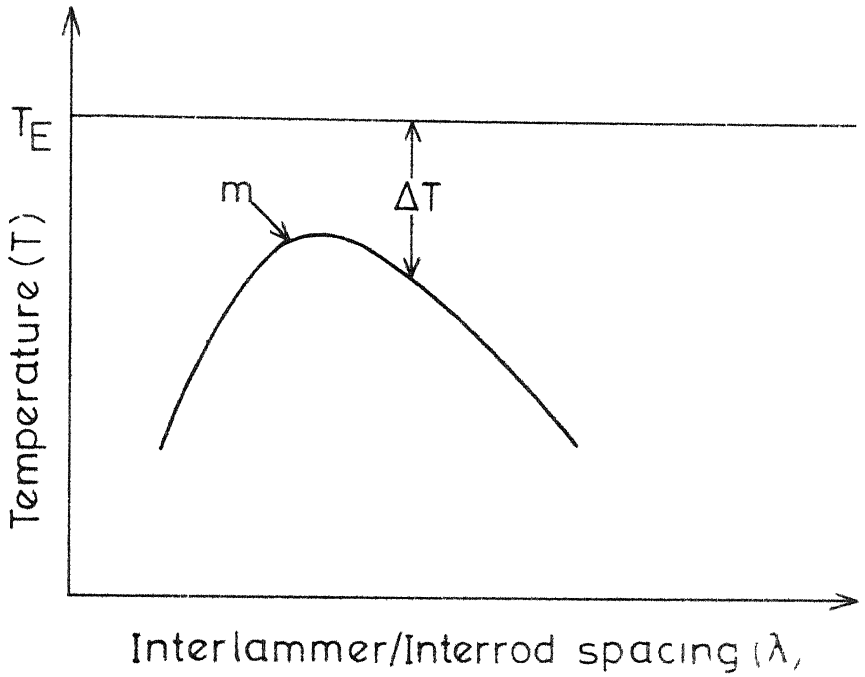

Fig. 6a. Change of interface temperature with lamellar spacing at constant growth rate.

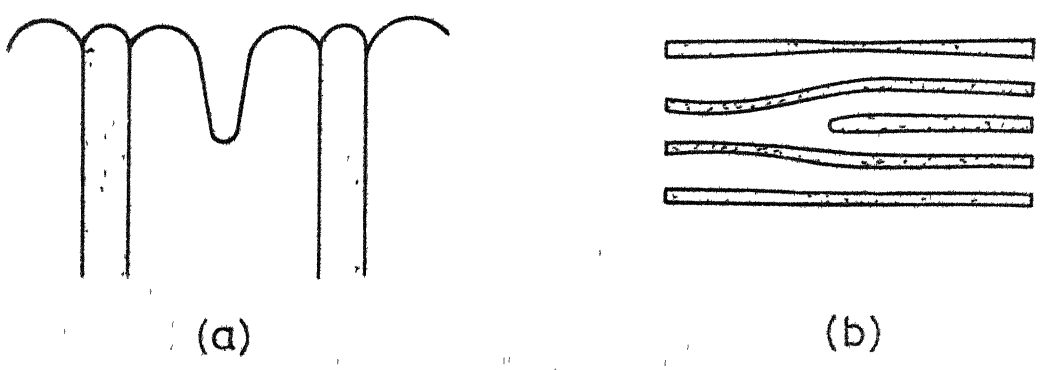

Fig. 6b. Schematic illustrations of mechanisms whereby plate spacing adjusts to increasing growth rate.

spacing is obtained.[9] Then how does nature decides which spacing to adopt? The simplest possibility is that growth is preferred at the extremum (m), i.e. minimum undercooling for a given velocity or equivalently maximum velocity for a given undercooling. This is represented by point m on the curve in Fig. 6. With this condition, maximization of the above equation gives a complete solution; that is

$$\lambda^2 \cdot V = \frac{B}{A} = \text{Const.}$$

$$\frac{T^2}{V} = 4AB = \text{Const.}$$

Experiment, on eutectic spacing invariably show $\lambda^2.V$ is a constant as predicted.[9]

Although there is not complete agreement among investigators yet as to how nature choose a lamellar spacing or undercooling at a given growth rate, certain limits can be specified as to how far λ can stray from the extremum condition.

The ways in which spacing gets adjusted are illustrated in Fig. 6. As pointed out by Jackson and Hunt[4] spacings smaller than at the extremum are inherently unstable and thus the extremum spacing is expected to be the minimum observed. Spacings somewhat larger than the extremum are not obviously unstable.

2.8 Solid Composition at Eutectic Front

The liquid composition at the eutectic front is just that of eutectic but the composition of the two phase solid forming there is not. It's exact average composition C_S^- depends on $\frac{G}{V}$,[8] where G is the temperature gradient in the liquid-solid region. Thus by writing a mass balance at the eutectic front for steady state solidification we get;

$$\left(\frac{dC_L}{dx'}\right)_{x'} = -\frac{V}{D_L}\left(C_E - C_S^-\right)$$

The two phase solid forming is of composition C_S^- and is different from C_E by an amount which balances the solute flux down the gradient $\left(\frac{dC_L}{dx'}\right)$. But $\left(\frac{dC_L}{dx'}\right)_{x' = 0} = \frac{G}{m_L}$.

where m_L = liqudus slope.

Therefore we can write

$$\overline{C}_S = C_E + \frac{D_L \cdot G}{m_L \cdot V}$$

Thus $\overline{C}_S = C_E$ at low values of $\frac{G}{V}$ and as $\frac{G}{V}$ increases it approaches C_o as a limit where C_o is the original composition of alloy.

CHAPTER 3

UNIDIRECTIONAL SOLIDIFICATION PROCESS

3.1 Apparatus

The apparatus used for unidirectional solidification in the present study is a modified version of the Stockbarger's method.(1) In this arrangement the sample is kept stationary on separate pedestal which is not connected with the main drive system. This way vibrational effects are minimised and we can expect a stable S/L interface.

The copper chill controlls the required unidirectional heat flow. Water cooling arrangement is provided to withdraw the heat effectively for maintaining high thermal gradient along S/L interface. The rate of heat extraction can be controlled by varying the flow of water through chill. With this method no intensive mold heating is necessary. This is due to the fact that the mold remains already at high temperature when surrounded by furnaces.

The two furnaces F_1 and F_2 with baffle plate are attached to a lead nut and a sliding bush. The lead screw can be rotated in either direction to raise and lower the furnace on the guide. The lead screw is journalled in a

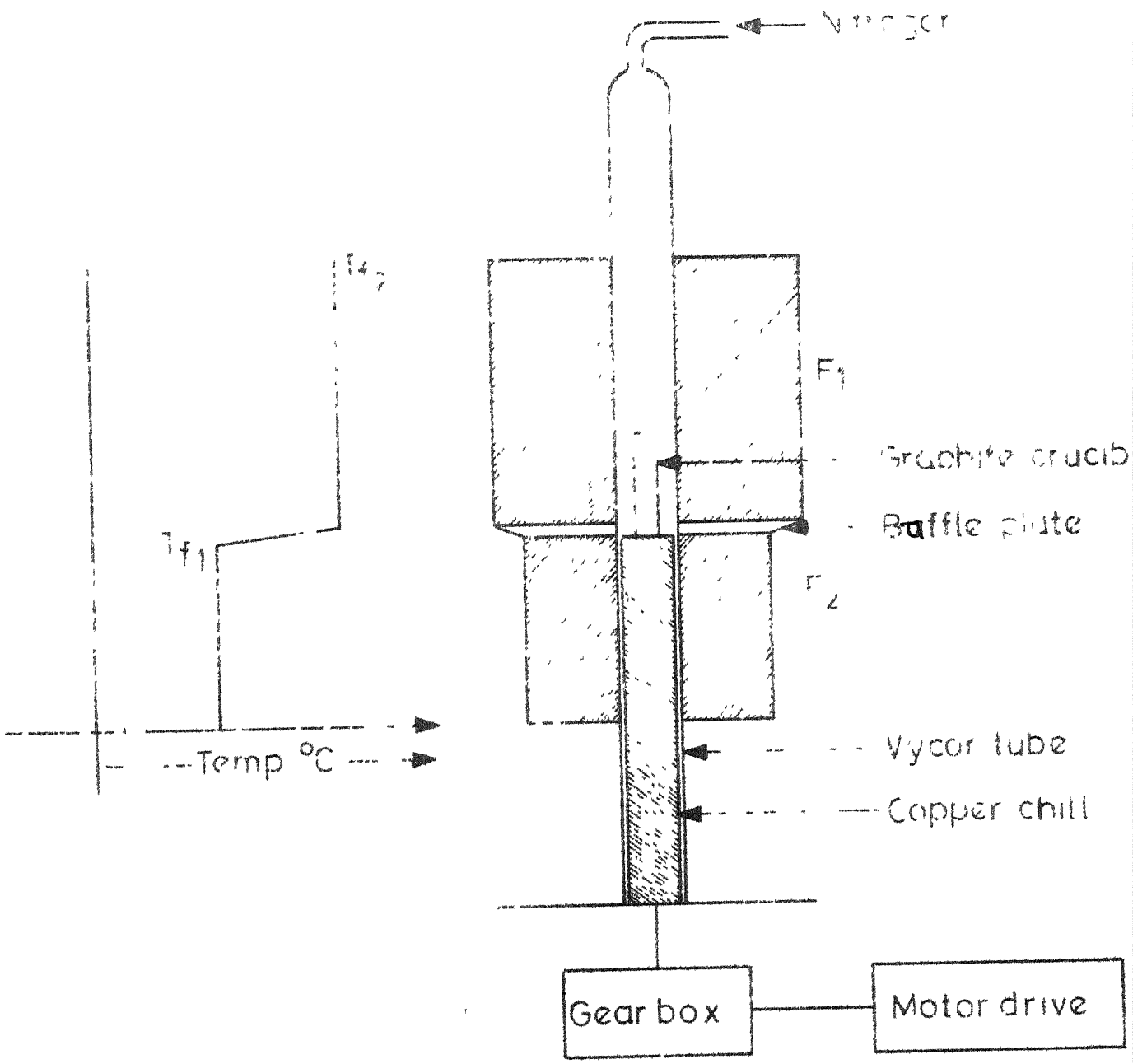

Fig. 7. [illegible] diagram of an apparatus for unidirectional [illegible] tion used in present study.

thrust bearing on the massive bed plate which also carries the guide. The chill is set up on a separate base plate.

3.2 Solidification Procedure

The constituents Al (99.995%) and 5.7 wt. % Ni (99.99%) were melted in induction furnace; under argon atmosphere. The alumina crucibles were used. The phase dia of Al-Al_3Ni eutectic is shown in Fig. 8. Induction melting is done at 1200°C for about half an hour to make sure that Ni gets completely diffused.

The alloys were remelted in air and cast into graphite molds as shown in Fig. 7. The samples obtained this way were unidirectionally solidified with the following condition:

T_{F_1} = 662°C , T_{F_2} = 625°C

Baffle thickness = 0.5 cm.

Thermal gradient (G_L) = 74°C/cm

Growth velocities — 1.5, 2, 2.5 cm/hr.

The solidified specimens were cut to yield longitudinal and transverse sections conventional optical metallographic techniques were used. Specially developed etching reagent by trial and error (0.5% aqueous hydrofluoric acid) was used. The microstructures are shown in Fig. 9.

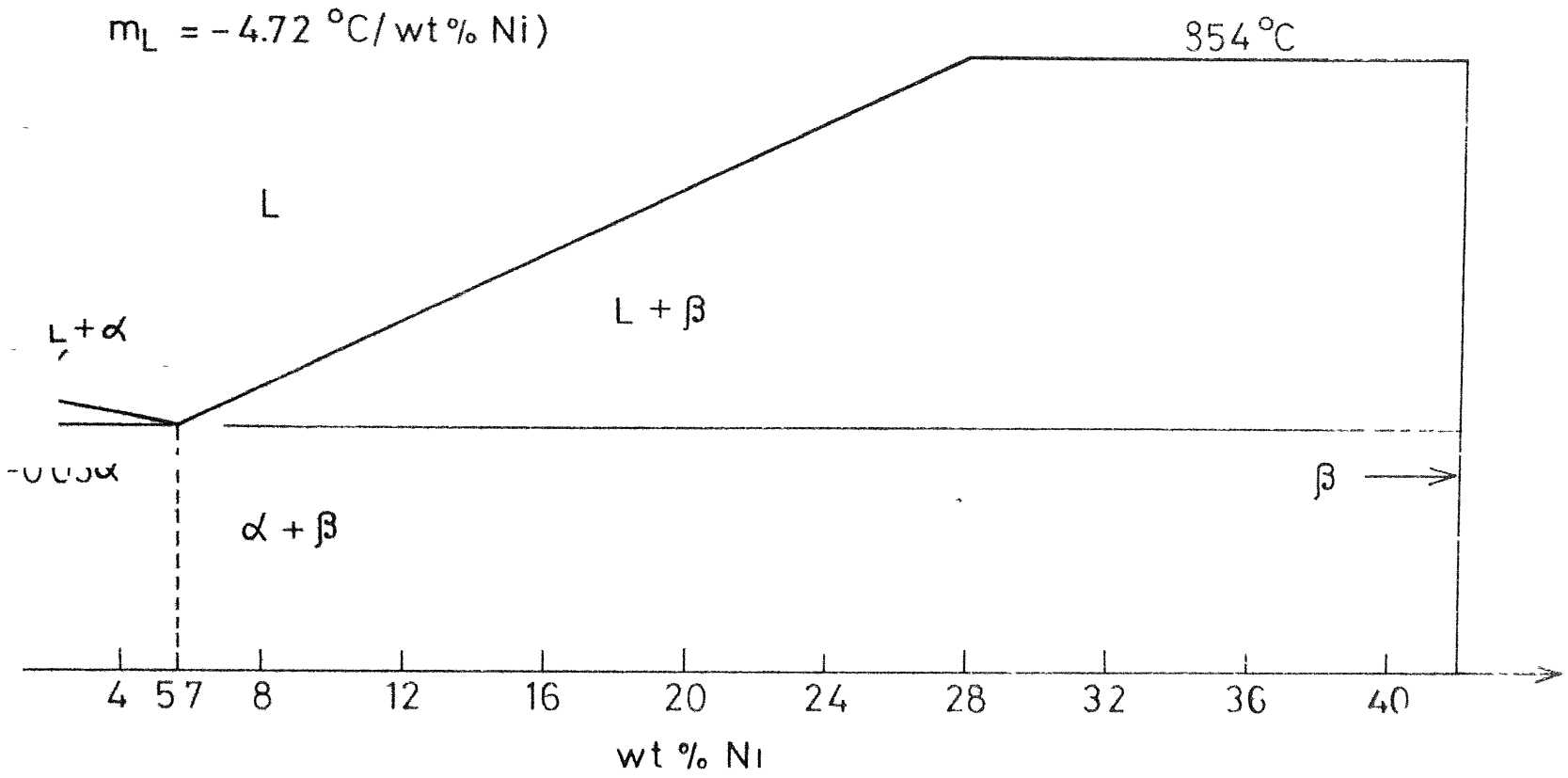

Fig. 8. Phase diagram for Al-Al_3Ni system.

Longitudinal section
M X 400

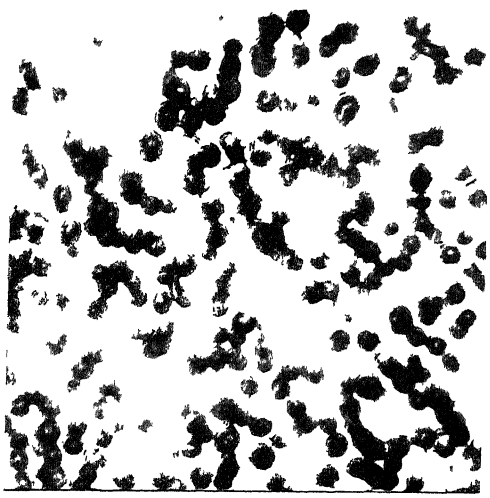

Transverse section
M X 400

Fig. 9a. Microstructures of directionally solidified alloys at V = 1.5 cm/hr; G = 74°C/cm.

Longitudinal section
M X 250

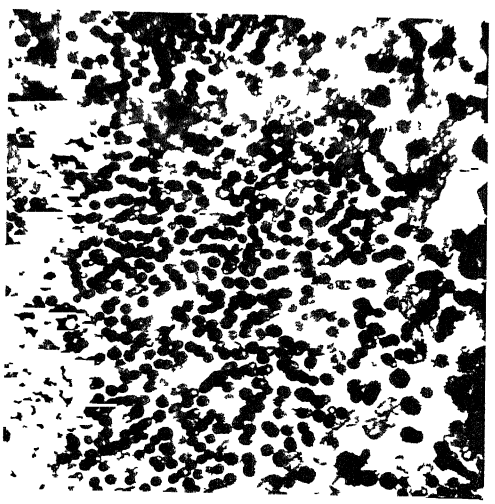

Transverse section
M X 250

Fig. 9b. Microstructures of directionally solidified alloys at V = 2 cm/hr; G = 74°C/cm.

Longitudinal section
M X 200

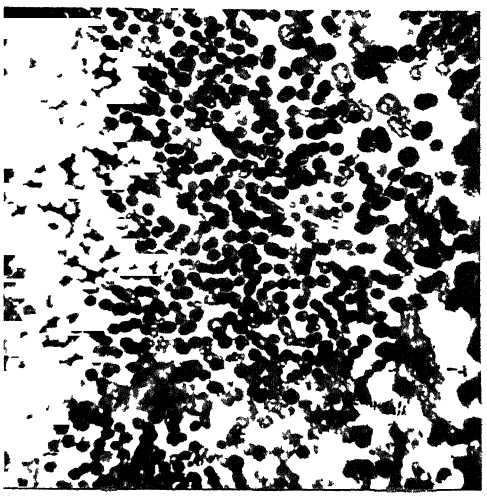

Transverse section
M X 200

Fig. 9c. Microstructures of directionally solidified alloys at V = 2.5 cm/hr; G = 74°C/cm.

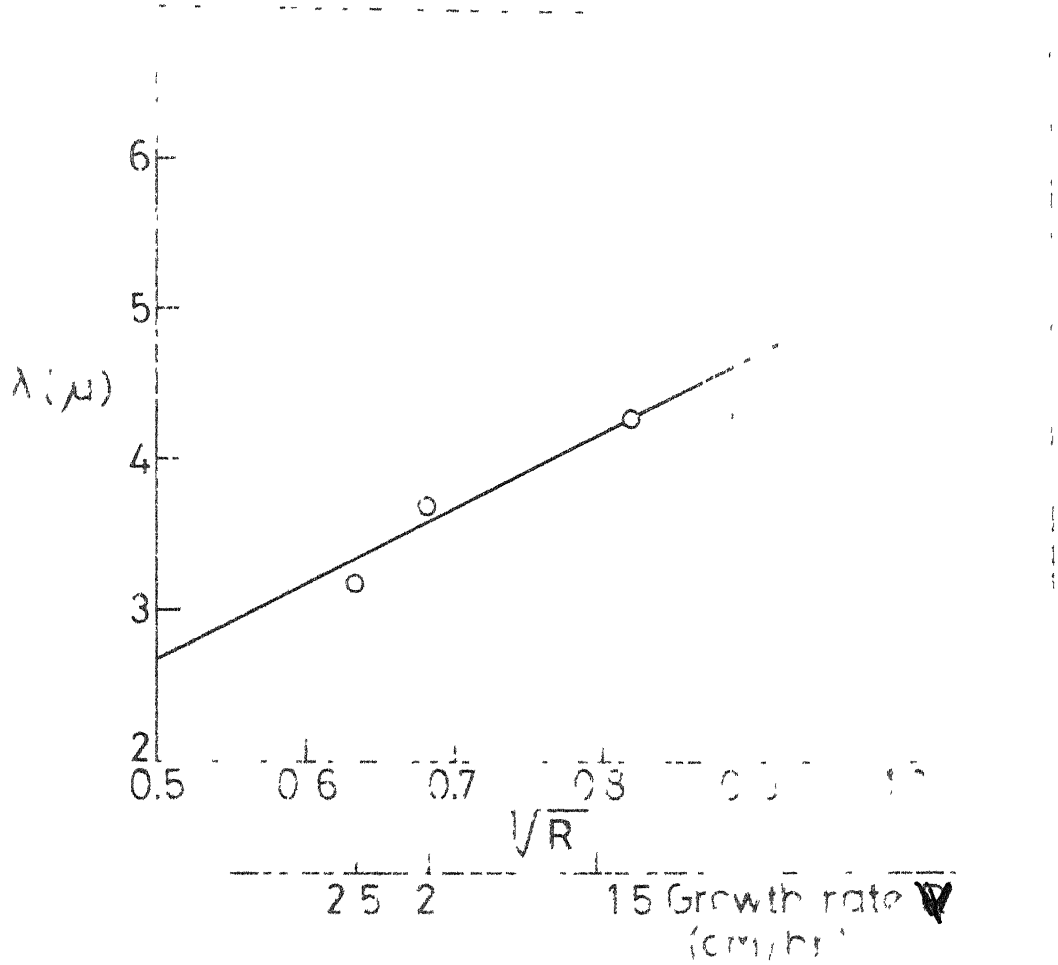

Fig. 10. Inter-rod spacing (λ) as a function of growth rate (V).

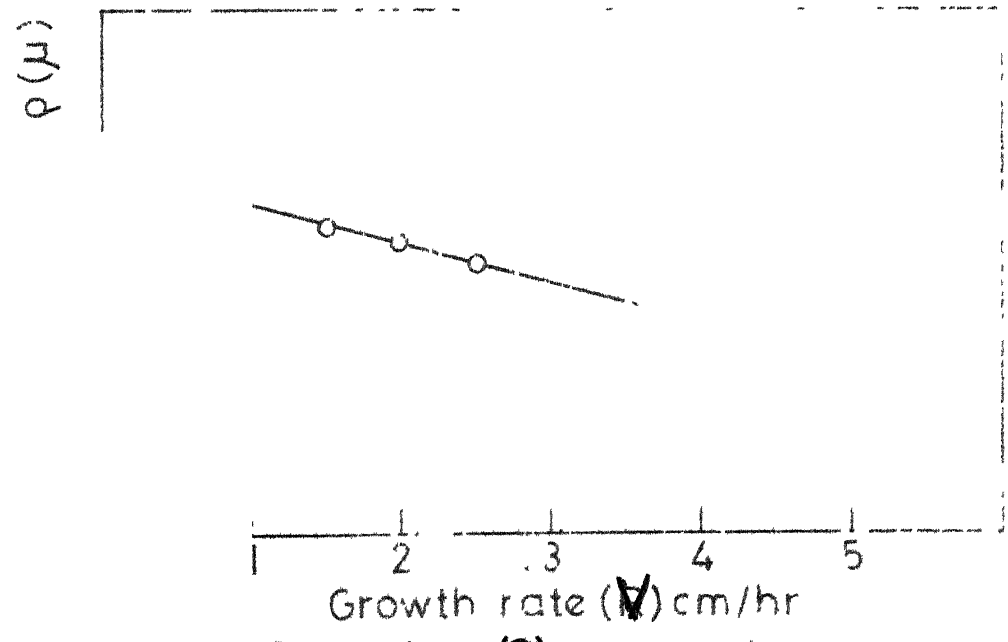

of curvature (ρ) as a ... on of growth rate

3.3 Results

The interrod spacing (λ) and tip radius of curvature (ρ) are measured as a function of growth velocity (V). The results are shown in Fig. 10 and 11. From Fig. 11 it is obvious that $\lambda^2 . V$ is almost constant. Experimental measurement of the radius (ρ) were made by magnifying the microstructures approximately 1200X. The interrod spacing and radius of curvature values are obtained by averaging from about 50 measurements in the same structure.

CHAPTER 4

ELECTRON PROBE MICRO-ANALYSIS

4.1 Introduction

The structure and properties of materials in physical metallurgy are very strongly influenced by composition and the distribution of the various constituents present in the material. The composition can be determined quantitatively to a high degree of accuracy and on a routine basis, using chemical, spectroscopic, and X-ray fluorescence techniques, while the identification of second phases can be carried out by standard X-ray diffraction techniques. Until the development of the electron-probe microanalyzer, however, there was no satisfactory way of determining the distribution of the various constituents in the material on a micron scale.

The basic concept of the electron probe is simple. A beam of electrons, approximately $\frac{1}{2}\mu$ in diameter strikes the specimen surface, interacting with atoms of the specimen to produce X rays. By measuring the wavelength and intensity of the X-rays produced, it is possible to determine which elements are present in the sample and their respective concentrations.

All microprobes currently available have the following main components:

(1) Electron optics to produce a small-diameter electron beam. This consists of an electron gun plus two electron lenses.

(2) One or more X-ray spectrometers to measure the wavelength and intensity of the characteristic X radiation produced.

(3) A light microscope to locate the area in the specimen to be examined.

Both the electron optics and the X-ray spectrometers operate at a vacuum of $\approx 10^{-4}$ Torr to prevent air molecules from absorbing the electrons and X-rays.

4.2 Specimen Preparation

During the directional solidification process the sample is removed from the apparatus and air quenched to arrest the interface. The specimen is cut, mounted on bakelite and silver painted to make the specimen conducting. Specimen must be conducting to prevent build up of heat or electric charge. The transverse sections analysed in this experiment were taken about 3-4 mm. below the final liquid-solid interface, and the error due to this is neglected. Following metallographic examination of specimens, regions

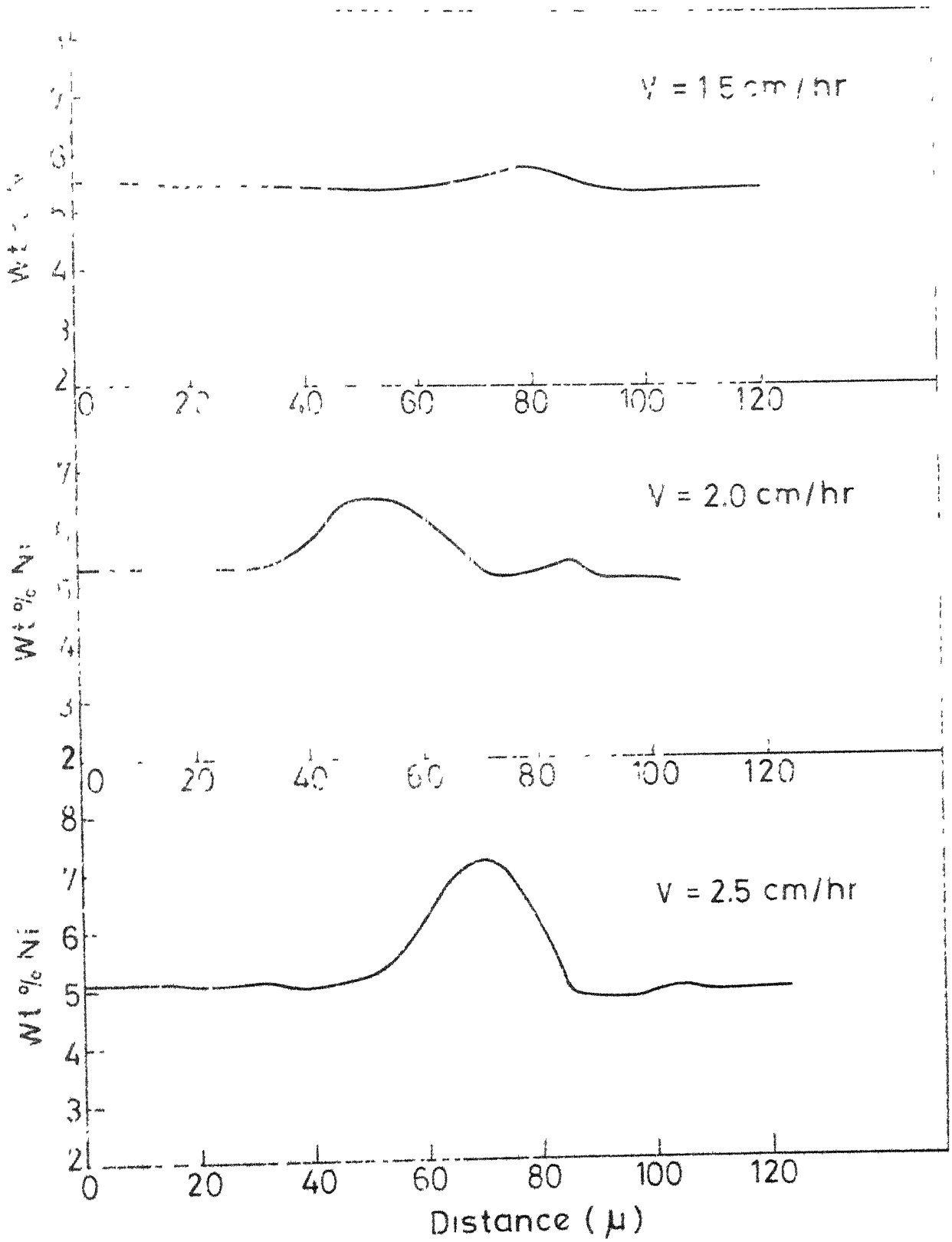

12. Electron probe microanalysis.

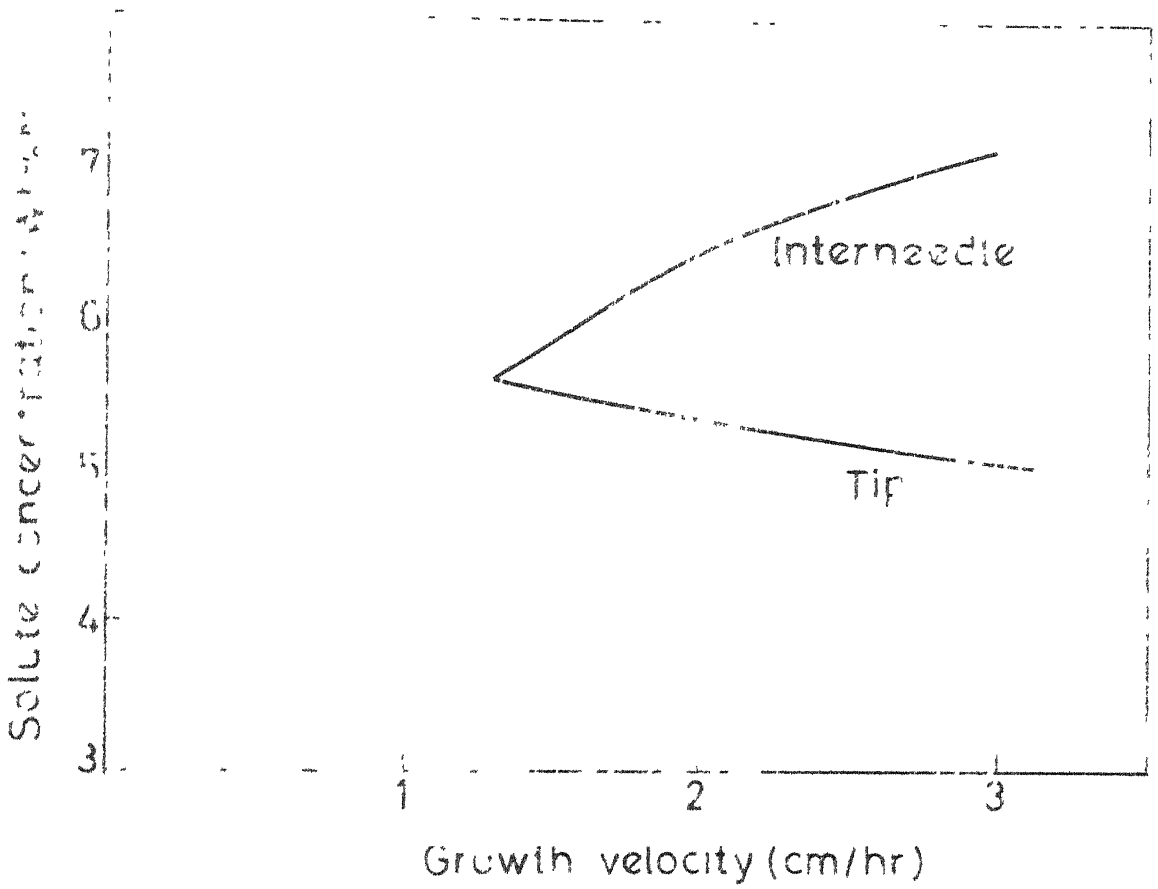

Fig. 13. Experimentally determined tip composition (C^{S}_{tip}) and interneedle region concentration as a function of growth rate (V) with constant thermal gradient (G) = 74°C/cm.

were selected for micro-analysis so as to scan across the centre of Al_3Ni precipitate. Etching is avoided as it can affect the surface composition.

4.3 Micro-Analysis Results

The concentration profile of Ni is determined using ACTON-CAMECA micro-analyzer. Accelerating voltage of 20 kV and specimen current of 160 μA are maintained. Counts are measured for 10 sec. along the cross section of whisker. Then by comparing these number of counts with counts for standard in sample; Ni concentration is calculated. Micro-analytical results are summarized in Fig. 12. From the data in Fig. 12, the minimum concentration at the tips and the maximum at the centre of whisker are plotted as a function of growth velocity (Fig. 13).

CHAPTER 5

TIP COMPOSITION AND TEMPERATURE PREDICTIONS

The treatment presented in this chapter is the modified form of Ivanstov's[3] approach for dendritic growth. The modification is done in the initial equation itself by restricting the growth in one direction only. Purdy[5] predicted tip composition and temperature for Fe - 8 wt.-% Ni system in which columner grains are observed. Here the efforts are made to extend the treatment for Al-Al_3Ni eutectic in which Al_3Ni whiskers are embedded in Al matrix.

The steady state shape of the interface of whisker tip is approximated by a paraboloid of revolution. The co-ordinate system is shown in Fig. 14. The basic equation for heat flow conduction is of the form[1]

$$\Delta^2 u = k \cdot \frac{\partial u}{\partial t} \qquad (1)$$

where $\Delta^2 = \frac{\partial^2}{\partial x^2} + \frac{\partial^2}{\partial y^2} + \frac{\partial^2}{\partial z^2}$

k = constant

t = time variable.

The equation (1) in the moving co-ordinate system takes the form (refer Appendix II).

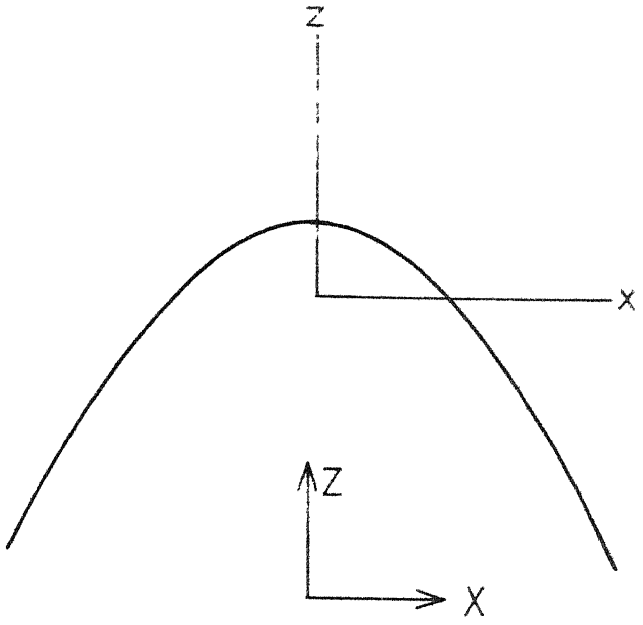

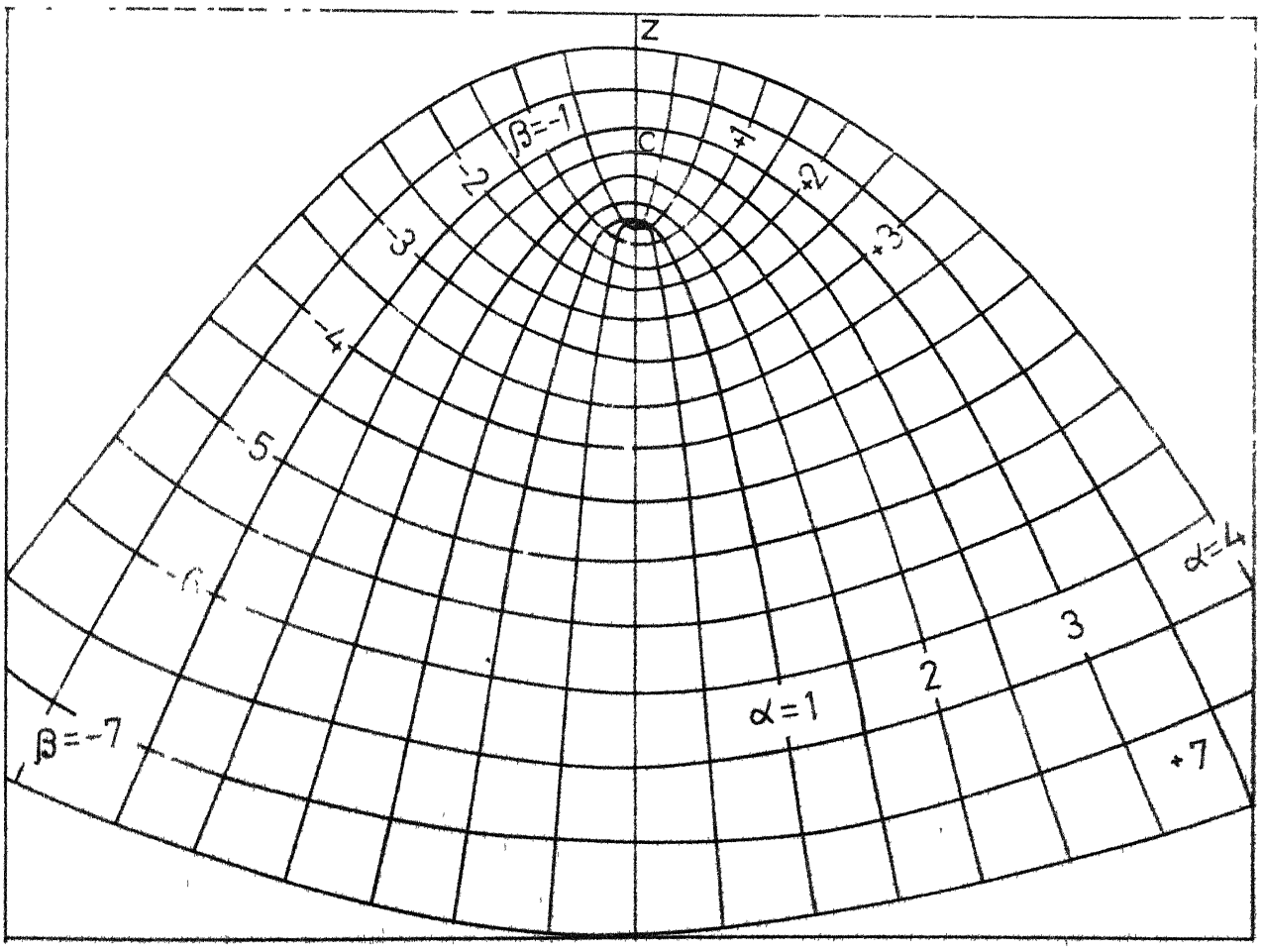

Fig. 14. Parabolic coordinate system.

$$\Delta^2 u = -k \cdot V \cdot \frac{\partial u}{\partial z} \qquad (2)$$

where V = growth velocity.

The eqn. (2) in the parabolic co-ordinates (α, β, ϕ) can be written with the help of following transformations[2] (refer Appendix III).

$$z = \frac{\beta^2 - \alpha^2}{2}$$

$$x = \alpha \cdot \beta \cdot \cos\phi \qquad (3)$$

$$y = \alpha \cdot \beta \cdot \sin\phi$$

Thus the equation (1) in parabolic co-ordinates takes the form (refer Appendix III).

$$\frac{\partial^2 u}{\partial \alpha^2} + \frac{\partial^2 u}{\partial \beta^2} + \left(\frac{1}{\alpha} - P \cdot \alpha\right)\frac{\partial u}{\partial \alpha} + \left(\frac{1}{\beta} + P \cdot \beta\right)\frac{\partial u}{\partial \beta} = 0 \qquad (4)$$

where $P = \frac{k.V}{2}$ and u some variable.

Now let us apply the general equation (4) for whisker growth. Considering the whisker tip as paraboloid of revolution growing into z direction as marked on the parabolic co-ordinate system (Fig. 14). The P in the above case is defined as Peclet number for our purpose and is a dimensionless parameter = $\frac{V.}{2D}$.

where V = growth velocity,

ρ = tip radius

D = diffusivity of Ni in Al at higher temperature.

The general solution of equation (4) is obtained as[5]

$$u(\alpha, \beta) = \sum_{n=o}^{\infty} E_n \frac{e^{-P}.\alpha^2 \; U(n+1,\ 1,\ P\alpha^2)}{e^{-P}\; U(n+1,\ 1,\ P)} \cdot Ln(P.\beta^2) \qquad (5)$$

where $U(a, b, x)$ = confluent hypergeometric function

$Ln(x)$ = Lagurre polynomial

E_n = arbitrary constant given by Purdy[5] which can be found out by boundary conditions

$$E_n = (C_{tip} - \frac{2T_m \cdot \gamma}{m \cdot \rho \cdot L} - C_\infty) \frac{(-1)^n}{\sqrt{n+1} \cdot \sqrt{-n+1}}$$

$$- \frac{G \cdot D}{m \cdot V} \cdot \frac{(-1)^n}{\sqrt{n+1} \cdot \sqrt{-n+2}}$$

$$+ \frac{2T_m \cdot \gamma}{m \cdot \rho \cdot L} P.e^P.I_{2n+1} \cdot erfc(\sqrt{P})$$

$$+ \frac{1}{m} \left(\frac{T_m \cdot \gamma}{\rho \cdot L} \cdot p^{\frac{1}{2}} \cdot e^P \frac{\sqrt{n+\frac{1}{2}}}{\sqrt{n+1}} \cdot I_{2n}\ erfc.(\sqrt{P}) \right) \qquad (6)$$

where x = gamma function.

$I_m.erfc(x)$ = normalized integral error function.

The final expression for C_{tip} takes the form as

$$C^{s}_{tip} = \frac{1}{2P}\left\{\frac{2(C_o - C_\infty)}{e^{P} \cdot E_1(P)} - \frac{V}{\mu_o} N_1(P) - C_o.V.N_L(P) + C_p\right\} \quad (7)$$

where N_1 and N_2 are defined in Appendix V:

where

C_∞ = initial composition of solute

C_o = equilibrium solute concentration in matrix

C_p = equilibrium solute concentration in precipitate

C_{tip} = actual concentration in matrix at the tip of precipitate.

The expression for interface undercooling can be written as

$$T = m.C_{tip} + \frac{2T_m \cdot \gamma \cdot V}{D \cdot \rho \cdot L} + \frac{V}{\mu_o} \quad (8)$$

Application to $Al-Al_3Ni$ system

The equations (7) and (8) are now applied to calculate (C^{S}_{tip} and undercooling ($T = T_{tip} - T_m$). The necessary parameters required for calculations are given below.

k_o = equilibrium partition coefficient from thermodynamic data[8,11] = 0.11

m = liquidus slope from Fig. 8 = - 4.72°C/wt. %

T_M = 913°K (640°C)

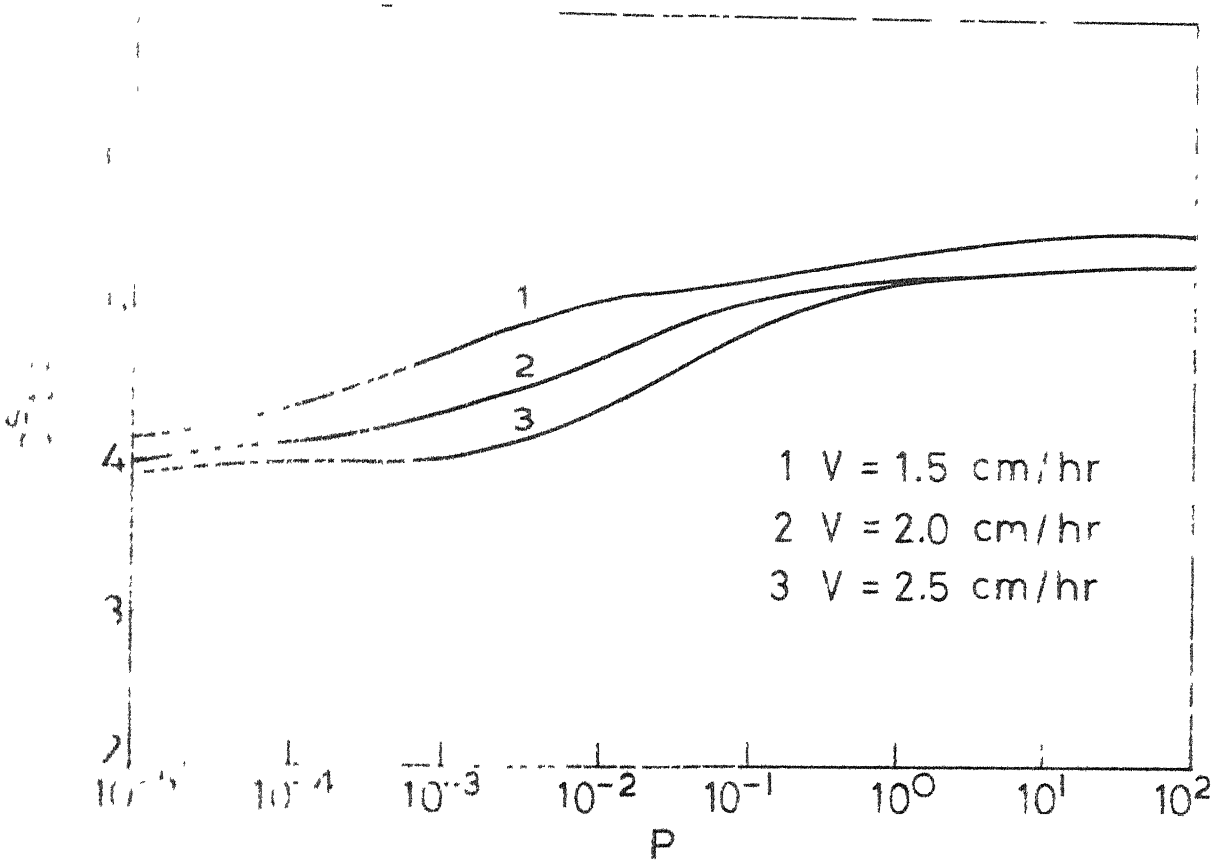

Fig. 15. Tip concentration (C^{S}_{tip}) as a function of (Peclet no.) (P) for several velocities.

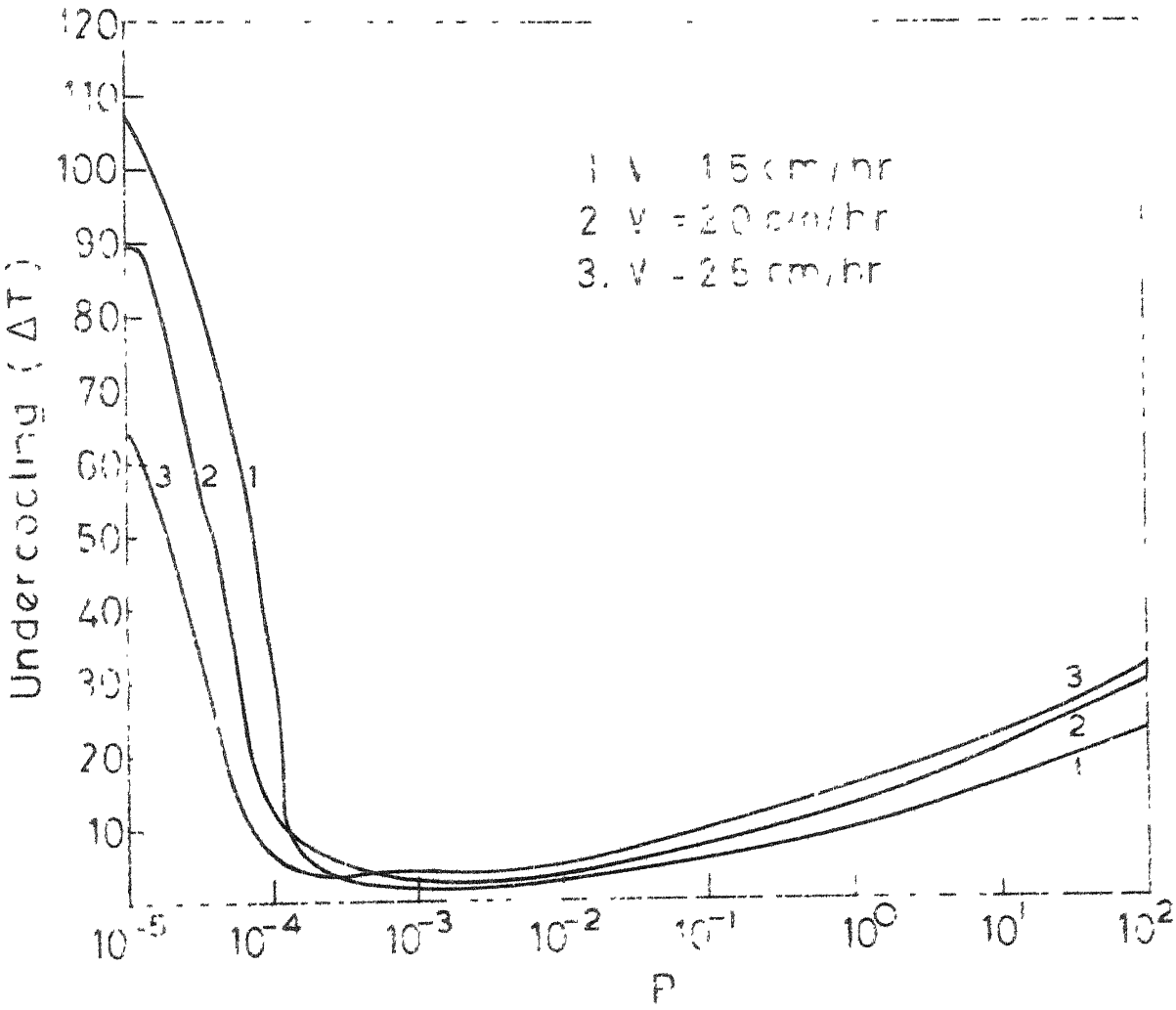

Fig. 16. Tip undercooling (ΔT) as a function of Peclet no. (P) for several velocities.

γ (Interfacial energy) = $2.2X10^{-5}$ cal/cm^2

D $5X10^{-5}$ cm^2/sec.

G = 74°C/cm (experimentally imposed condition)

d = 2.7 gm/cm^3 density of Al

k = 0.06 cal/sec-cm-°K

L = 253 cal/cm^3

C = 5.7 wt. % Ni

C_p = 42 wt. % Ni in Al_3Ni whisker

The standard tables are available for the quantities involved in the above equations.[1,2,4,11,12,13] The results are shown in Fig. 15 and 16.

CHAPTER 8

DISCUSSION AND CONCLUSIONS

8.1 Growth Velocity Bounds:

According to the relation $\lambda^2 . V = \text{Constant}$, higher growth velocity gives lower λ i.e. fine structure and effectively gives better mechanical properties. Thus high growth velocity is desirable. But there is V_{max} beyond which some practical difficulties arise.

Considering heat balance at a planar L/S interface from melt

$$K_S \cdot G_S - K_L \cdot G_L = \rho_S \cdot H \cdot V$$

where

K_S, K_L = Thermal conductivity of solid and liquid respectively.

G_S, G_L = Thermal gradient in solid and liquid.

ρ_S = Density of solid.

H = Heat of fusion.

V = Growth velocity.

Thus V would be maximum when G_L is negative (under cooled melt). However good whiskers can not be grown with under-cooled melt as dendrites will be formed there. The

practically maximum possible growth velocity corresponds to $G_L = 0$.

$$\therefore \quad V_{max} = \frac{K_s \cdot G_s}{\rho_s \cdot H}$$

Also at higher growth velocities the problem of heat dissipitation exists due to the difficulty in maintaining unidirectional heat flow. Moreover, maintaining higher G_L in order to get plane front solidification is not practicable.

Lower growth velocities are used, as even with low G_L, plane front can be maintained. But the spacing get increased and mechanical properties are deteriorated. Thus the proper selection of growth velocity is essential keeping the above points in mind.

8.2 Comparison of Present Calculations with Ivanstove's Approach for Dendrites:

Ivanstove approximated the shape of isolated dendrite interface of paraboloid of revolution moving in the direction of growth. He accounted for cross branching and coarsening of dendrites and formulated the heat flow equation in parabolic co-ordinates.

Here we have considered isolated whisker (cell) interface also as a paraboloid of revolution but no cross

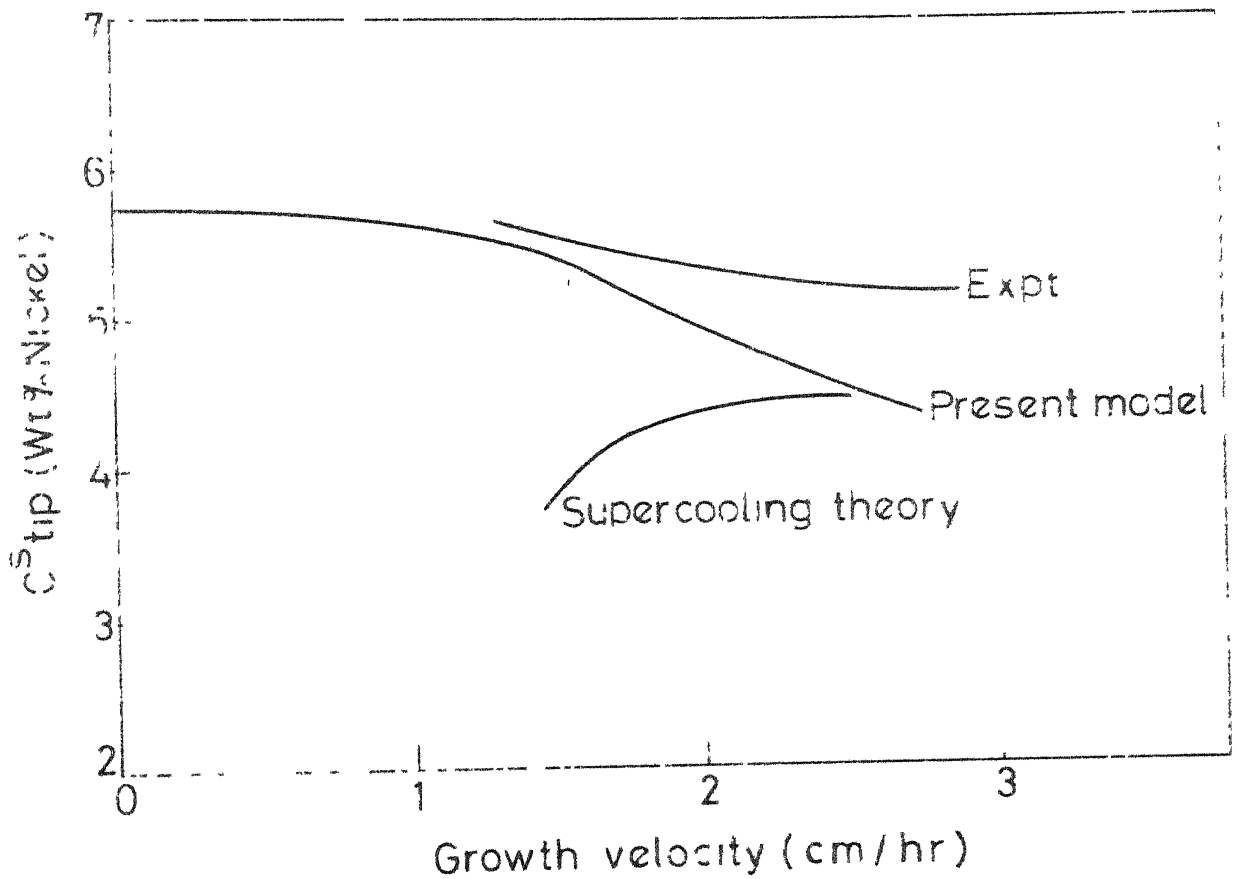

Fig. 19. Comparison of experimentally determined C^{S}_{tip} with present model and zero constitutional supercooling theory.

boundary and coarsening has been accounted due to their nonexistence. Thus we get simplified version of heat flow equation in moving parabolic co-ordinate system. The problem becomes extremely complicated if we try to consider the effect of other growing cells on the cell under consideration. As this effect is neglected and due to other assumptions as studied in the text the predicted values are approximate. But still the results are well in agreements with the values obtained by Electron-Probe Microanalysis (Fig. 20). The results by zero constitutional supercooling criterion are also presented in Fig. 20. The validity and merit of present approach is thus justified.

8.3 Conclusions:

(1) Treatment has been developed to describe approximately the steady controlled solidification of a dilute binary alloy. The precipitate tip has been represented by a paraboloid of revolution. This assumption reduced a complex free boundary problem to a simpler one with the consequent reduction of generality.

(2) The effect of neighbouring dendrites or needles should be taken into account in future work.

(3) For a fixed temperature gradient the predicted tip concentration decreases rapidly in low velocity regime as compared to the high velocity regime.

(4) The experimental values of tip concentration are in reasonable accord with the predicted values. In contrast predictions based on the principles of zero constitutional supercooling are in strong disagreement with the present observation. We consider that the zero constitutional supercooling principle is inappropriate to the unidirectional solidification problems and that they should be replaced by the unwildy but more correct extremum principle employed in this work.

BIBLIOGRAPHY

Chapter 1

1. R.W. Kraft, D.L. Albright; Trans. A.I.M.E., 95 (1961) p. 221.
2. F.D. Lemkey, R.W. Hertzberg and J.A. Ford; Trans. A.I.M.E., 233 (1965) p. 342.
3. M.J. Salkind, B.T. Bayles, F.D. George and W.K. Tice; "Investigation of fracture mechanisms, thermal stability and hot strength properties of controlled polyphase alloys", Final report contract no. W 64-0433-d, March 12, 1965.
4. R.W. Kraft, D.L. Albright and J.A. Ford; Trans. A.I.M.E., 227 (1963) p. 540.
5. G.J. May; Metals and Materials, Sept. (1975).
6. G.J. May and Jones; Metals and Materials, 8 (1974).

Chapter 2

1. J.D. Hunt and K.A. Jackson; Trans. A.I.M.E., 236 (1966) 843.
2. J.D. Hunt and K.A. Jackson; Trans. A.I.M.E., 236 (1966) 1129.
3. G.J. Davies; "Solidification and Casting", Applied Science Publishers Ltd., London, 1973.

4. M.G. Day and A. Hellawell; Proc. of Royal Society, A.305 (1968) 473.
5. A. Hellawell; Met. and Materials, 1 (1967) 361.
6. Cooksey, Munson, Wilkinson and Hellawell; Phil. Mag., 10 (1964) 745.
7. W.A. Tiller; "Polyphase Solidification", Seminar on liquid metals and solidification, ASM, Cleveland, Ohio.
8. M.C. Flemings; "Solidification Processing", Mc-Graw Hill Series in Mat. Sci. and Engg.
9. M. Flemings; Trans. A.I.M.E., 239 (1967) 1534.

Chapter 3

1. Chester T. Sims and Hagel; "The Superalloys", A Wiley Interscience Publication, 1972.
2. R.W. Kraft and D.L. Albright; Trans. A.I.M.E., 221 (1961) 95.
3. M. Hanjen, "Constitution of binary alloys".

Chapter 4

1. Martin and Pool,
Metals and Materials, 14 (1969) 133, Review article.
2. F. Weinberg, "Tools and Techniques in Physical Metallurgy", Marcel Dekker, Inc., New York, 1970.

Chapter 5

1. F.B. Hildebrand, "Advanced calculus for applications", Prentice Hall, Inc., New Jersey (1963).
2. H. Margenau and G.M. Murphy, "The Mathematics of Physics and Chemistry", East West Press, New Delhi (1971).
3. G.P. Ivanstov, Dokl. Akad. Nauk, SSSR 58 (1967) 567.
4. R. Trivedi, Acta. Met., 18 (1970) 287.
5. G.R. Purdy, J. Crystal Growth, (1974) 29.
6. D.E. Temkin, Dokl. Akad. Nauk. SSSR 58 (1960) 1307.
7. E.G. Holzmann, J. Appl. Phys., 41 (1970) 1460.
8. M.C. Flemings, "Solidification Processing", McGraw Hill Series in Mat. Sci. and Engg., p. 272.
9. K.A. Jackson and J.D. Hunt, Trans. A.I.M.E. 236 (1966) 1129.
10. Bateman, "Tables of Integral Transforms", Bateman manuscript, Vol. 1.
11. Hultgren and others, "Selected values of thermodynamic properties of metals and alloys", 1963, John Wiley and Sons, Inc.
12. P.R. Garbedian, "Partial differential equation",
13. B.S. Berryland and others, Tables of integral error functions and polynomial".

Chapter 6

1. R.W. Hertzberg, Lemekey, Ford, Trans. A.I.M.E. 233 (1965) 342
2. Jones, Metals and Materials.
3. G.A. Chadwick, Prog. Mat. Sci., 12 (1963) 97.
4. May and Chadwick, Metal Sci. Journal, 2 (1973) 20.
5. H. Weiss, Met. Trans., 2 (1971) 1513.

General

1. R.C. Barclay and Winegard, Mat. Sci. and Engg., 13 (1974) 291.
2. A.J. Perry, Mat. Sci. and Engg., 11 (1973) 203.
3. W. Oldfield, Mat. Sci. and Engg., 11 (1973) 211.
4. I. Stakgold, "Boundary value problems of mathematical physics", Vol. 2, 327.

APPENDIX I

OBSERVATION TABLES

Table I.1 Velocity, spacing, tip radius measurements.

Growth velocity (cm/hr)	1.5	2	2.5
Growth velocity (cm/sec.)	0.42×10^{-3}	0.56×10^{-3}	0.69×10^{-3}
Spacing (microns)	4.3	3.7	3.2
Tip radius (microns)	4.0	3.9	3.5
$P = \frac{V.\rho}{2D}$	1.68×10^{-2}	2.18×10^{-2}	2.41×10^{-2}

Table I.2 Electron probe micro-analysis.

Distance (microns)	Weight % Ni		
	V = 1.5 cm/hr	V = 2 cm/hr	V = 2.5 cm/hr
0	5.5	5.3	5.1
20	5.5	5.3	5.1
40	5.5	5.8	5.0
60	5.4	6.2	6.2
80	5.8	5.1	6.0
100	5.4	5.1	4.9
120	5.4	-	4.9

Table I.3 Calculated C^S_{tip} and ΔT values.

I.3.1 Growth velocity V = 1.5 cm/hr

P	10^{-5}	10^{-4}	10^{-3}	10^{-2}	10^{-1}	10^{0}	10^{1}	10^{2}
C^S_{tip}	4.20	4.35	4.65	5.1	5.2	5.45	5.55	5.55
ΔT	66.8	6.4	4.2	5.9	10.4	16.2	24.1	26.4

I.3.2 Growth velocity V = 2 cm/hr

P	10^{-5}	10^{-4}	10^{-3}	10^{-2}	10^{-1}	10^{0}	10^{1}	10^{2}
C^S_{tip}	3.9	4.05	4.35	4.7	5.1	5.1	5.3	5.35
ΔT	87.8	8.8	3.2	3.6	8.5	14.2	22.2	31.0

I.3.3 Growth velocity V = 2.5 cm/hr

P	10^{-5}	10^{-4}	10^{-3}	10^{-2}	10^{-1}	10^{0}	10^{1}	10^{2}
C^S_{tip}	3.90	4.0	4.35	4.9	4.95	5.1	5.3	5.35
T	108.8	11.8	3.0	2.1	9.3	13.8	20.8	30.9

N.B.: Here

C^S_{tip} — wt. % Ni; ΔT — °C, P — dimensionless number.

APPENDIX II

HEAT FLOW EQUATION IN MOVING CO-ORDINATES

Heat flow in steady state is of the form

$$\triangle^2 U = K \cdot \frac{\partial u}{\partial t}$$

let (x, y, z, t) represents steady co-ordinate system and (x', y', z', t') represents moving co-ordinate system. Thus applying Gallilian transformations we can write

$$z' = z - V \cdot t$$

$$x' = x$$

$$y' = y$$

$$t' = t$$

$$\frac{\partial}{\partial z} = \frac{\partial}{\partial z'}\frac{\partial z'}{\partial z} + \frac{\partial}{\partial t'}\frac{\partial t'}{\partial t} + \frac{\partial}{\partial y'}\frac{\partial y'}{\partial y} + \frac{\partial}{\partial x'}\frac{\partial x'}{\partial x}$$

$$= \frac{\partial}{\partial z'}\frac{\partial z'}{\partial z}$$

$$= \frac{\partial}{\partial z'} \quad \text{- - - -} \quad \left(\text{As } \frac{\partial z'}{\partial z} = 1\right)$$

Similarly

$$\frac{\partial}{\partial x} = \frac{\partial}{\partial x'}, \qquad \frac{\partial}{\partial y} = \frac{\partial}{\partial y'}$$

$$\frac{\partial}{\partial t} = \frac{\partial}{\partial t'}\frac{\partial t'}{\partial t} + \frac{\partial}{\partial z'}\frac{\partial z'}{\partial t}$$

$$= \frac{\partial}{\partial t'} - V \cdot \frac{\partial}{\partial z'} \quad - - - \left(\frac{\partial z'}{\partial t} = -V, \quad \frac{\partial t'}{\partial t} = 1\right)$$

$$= -V \frac{\partial}{\partial z}$$

$$\frac{\partial^2}{\partial x'^2} = \frac{\partial}{\partial x^2}, \quad \frac{\partial}{\partial y'^2} = \frac{\partial}{\partial y^2}, \quad \frac{\partial}{\partial z'^2} = \frac{\partial}{\partial z^2}$$

$$\frac{\partial}{\partial t} = -V \cdot \frac{\partial}{\partial z'}$$

Heat flow in moving co-ordinate takes the form

$$\frac{\partial^2 u}{\partial x'^2} + \frac{\partial^2 u}{\partial y'^2} + \frac{\partial^2 u}{\partial z'^2} = -k \cdot V \cdot \frac{\partial u}{\partial z'}$$

$$\therefore \quad \triangle'^2 u = -k \cdot V \cdot \frac{\partial u}{\partial z'}$$

For simplicity, remove primes

$$\therefore \quad \triangle^2 u = -k \cdot V \cdot \frac{\partial u}{\partial z}$$

APPENDIX III

CONVERSION OF HEAT FLOW EQUATION IN MOVING CO-ORDINATE EQUATIONS INTO PARABOLIC CO-ORDINATE SYSTEM

Let (α, β, ϕ) represent co-ordinates in parabolic system.

$$\therefore \quad z = \frac{\beta^2 - \alpha^2}{2}$$

$$x = \alpha \cdot \beta \cdot \cos\phi$$

$$y = \alpha \cdot \beta \cdot \cos\phi$$

Thus $$x^2 + y^2 = \alpha^2\beta^2$$

$$\tan\phi = \frac{y}{x}$$

On substitution we can write

$$x^2 + y^2 = 4\beta^4 - 4\beta^2 \cdot z$$

$$x^2 + y^2 = 4\alpha^2 z - 4\alpha^4$$

$\frac{\partial u}{\partial z}$ in parabolic system

$$\frac{\partial u}{\partial z} \equiv \frac{\partial u}{\partial \alpha} \cdot \frac{\partial \alpha}{\partial z} + \frac{\partial u}{\partial \beta} \cdot \frac{\partial \beta}{\partial z} + \frac{\partial u}{\partial \phi} \cdot \frac{\partial \phi}{\partial z}$$

But $$\frac{\partial \beta}{\partial z} = \frac{\beta^2}{4\beta^3 - 2\beta \cdot z}$$

$$\frac{\partial \alpha}{\partial z} = \frac{-\alpha^2}{2\alpha \cdot z + 4\alpha^3}$$

Substituting and neglecting $\frac{\partial \phi}{\partial z}$ in the expression for $\frac{\partial u}{\partial z}$; we can write

$$\frac{\partial u}{\partial z} = \frac{1}{2(\alpha^2 + \beta^2)} [- \alpha \cdot \frac{\partial u}{\partial \alpha} + \beta \cdot \frac{\partial u}{\partial \beta}]$$

$\Delta^2 u$ in parabolic system

Using the general form available for curvilinear co-ordinates(2)

$$\Delta^2 u = \frac{1}{\alpha^2 + \beta^2} [\frac{\partial^2 u}{\partial \alpha^2} + \frac{\partial^2 u}{\partial \beta^2} + \frac{1}{\alpha} \cdot \frac{\partial u}{\partial \alpha} + \frac{1}{\beta} \cdot \frac{\partial u}{\partial \beta} + \frac{\alpha^2 + \beta^2}{\alpha} \cdot \frac{\partial^2 u}{\partial \phi^2}]$$

Neglecting $\frac{\partial^2 u}{\partial \phi^2}$ as u is independent of ϕ and substituting for $\Delta^2 u$ and $\frac{\partial u}{\partial z}$ in the heat flow equation in moving co-ordinate system

$$\frac{\partial^2 u}{\partial \alpha^2} + \frac{\partial^2 u}{\partial \beta^2} + (\frac{1}{\alpha} - P \cdot \alpha) \frac{\partial u}{\partial \alpha} + (\frac{1}{\beta} - P \cdot \beta) \frac{\partial u}{\partial \beta} = 0$$

where $P = \frac{k \cdot V}{2}$.

APPENDIX IV

SOLUTION OF HEAT FLOW EQUATION

$$u(\alpha, \beta) = F(\alpha) \cdot G(\beta) \quad \text{(separation of variables)}$$

$$\frac{1}{F}\left[\frac{d^2F}{d\alpha^2} + \left(\frac{1}{\alpha} + 2P\alpha\right)\frac{dF}{d\alpha}\right] = -\frac{1}{G}\left[\frac{d^2G}{d\beta^2} + \left(\frac{1}{\beta} - 2P\beta\right)\frac{dG}{d\beta}\right]$$

The two equations can be formed as

$$\frac{d^2F}{d\alpha^2} + \left(\frac{1}{\alpha} + 2P\alpha\right)\frac{dF}{d\alpha} - F = 0 \qquad (1)$$

$$\frac{d^2G}{d\beta^2} + \left(\frac{1}{\beta} - 2P\beta\right)\frac{dG}{d\beta} + G = 0 \qquad (2)$$

$F(\alpha) = \psi\left(\frac{\lambda}{4P}, 1, P\alpha^2\right)$ -- comparing to standard form from reference 1 of Chapter 5

$G(\beta) = \psi\left(-\frac{\lambda}{4P}, 1, P\beta^2\right)$

$\approx L_n(P\beta^2)$ -- reference 1, Chapter 5

$$\therefore u(\alpha, \beta) = \sum_{n=0}^{\infty} \psi(n+1, 1, P\alpha^2) \cdot L_n(P\beta^2) \cdot C_n$$

where choose $C_n = \dfrac{E_n}{e^{-P} \cdot \psi(n+1, 1, P)}$

$$\therefore \psi(\alpha,\beta) = \sum_{n=0}^{\infty} E_n \cdot \frac{e^{-P\alpha^2}\, \psi(n+1, 1, P\alpha^2)}{e^{-P}\, \psi(n+1, 1, P)} L_n(P \cdot \beta^2)$$

APPENDIX V

OUTLINE TO CALCULATE C^{S}_{tip} AND $\triangle T$

N_1 and N_2 are defined as below.

$$N_1 = 2P^{3/2} \cdot e^{P} \cdot \sum_{n=o}^{\infty} \frac{\Gamma_{n+\frac{1}{2}}}{\Gamma_{n+1}} \cdot I_{2n} \cdot \operatorname{erfc}(\sqrt{P})$$

$$X \frac{\Psi(n+1,\ 2,\ P)}{\Psi(n+1,\ 1,\ P)} X\ L_n(P\beta^2)$$

$$N_2 = 2P^{3/2} \cdot e^{P} \cdot [\sum_{n=o}^{\infty} 2\sqrt{P}\ \pi\ I_{2n+1}\ X\ \operatorname{erfc}.\sqrt{P}$$

$$+ \frac{\Gamma_{n+\frac{1}{2}}}{\Gamma_{n+1}} \cdot I_{2n} \cdot \operatorname{erfc}\cdot\sqrt{P}]$$

$$X \frac{\Psi(n+1,\ 2,\ P)}{\Psi(n+1,\ 1,\ P)} \cdot L^{o}_{n}(P\beta^2).$$

$$C_{tip} = \frac{1}{2P} \frac{2(C_o - C_\infty)}{e^{P}\ E_1(p)} - \frac{V}{\mu_o} N_1(p) - C_o \cdot V \cdot N_2(p) + C_p$$

As $C_o = C_\infty$ the first term is o

$$\therefore C_{tip} = \frac{1}{2P} - \frac{V}{\mu_o} N_1(p) - C_o \cdot V \cdot N_2(p) + C_p$$

$C_p = 0.42, \quad C_o = 5.7$

Consider for $P = 10^{-5}$, $N_1 = 1.5$, $N_2 = 1.98$

$$\mu_o = 200, \quad V = 0.42X10^{-3} \text{ cm/sec.}$$

$$C_{tip} = \frac{1}{2 \cdot P}\left\{- \frac{0.42X10^{-3} \text{ X } N_1}{200} - 5.7X10^{-2} \text{ X } 0.42X10^{-3} \text{ X } N_2 + 0.42 \right\}$$

$$= \frac{1}{2 \cdot P}\left\{- 0.21X10^{-5}(N_1) - 0.24X10^{-5}(N_2) + 0.42 \right\}$$

$$= \frac{1}{P}\left\{- 0.105X10^{-5}(N_1) - 0.12X10^{-5}(N_2) + 0.42 \right\}$$

$$= \frac{1}{P}\left\{- 0.105X1.4X10^{-5} - 0.12X1.98X10^{-5} + 0.42 \right\}$$

$$= - 0.14 - 0.378 + 0.420$$

$$= 0.042$$

$$\therefore \quad C_{tip} = 4.2$$

$$\Delta T = m \cdot C_{tip} + \frac{2T_m \cdot \gamma \cdot V}{D \cdot P \cdot L} + \frac{V}{\mu_o}$$

$$\simeq 107^{o}C$$

ME-1976-M-BON-UNI